Journal of Materials Science: Materials in Medicine (2025)36:5
https://doi.org/10.1007/s10856-024-06849-0

BIOCOMPATIBILITY STUDIES

Original Research

Knockdown of decorin in human bone marrow mesenchymal stem cells suppresses proteoglycan layer formation and establishes a pro-inflammatory environment on titanium oxide surfaces

Hisanobu Kamio[1] · Kazuto Okabe[2] · Masaki Honda[3] · Kensuke Kuroda[4] · Shuhei Tsuchiya[2]

Received: 21 January 2024 / Accepted: 4 December 2024
© The Author(s) 2024

Abstract

Osseointegration is essential for successful implant treatment. However, the underlying molecular mechanisms remain unclear. In this study, we focused on decorin (DCN), which was hypothesized to be present in the proteoglycan (PG) layer at the interface between bone and the titanium oxide (TiOx) surface. We utilized DCN RNA interference in human bone marrow mesenchymal stem cells (hBMSCs) to investigate its effects on PG layer formation, proliferation, initial adhesion, cell extension, osteogenic capacity, fibrotic markers, and immunotolerance to TiOx in vitro. After 14 days of cultivation, we observed no PG layer was detected, and the osteogenic capacity was suppressed in DCN-depleted hBMSCs. Furthermore, the conditioned medium upregulated the expression of M1 macrophage markers in human macrophages. These results suggest that endogenous DCN plays a crucial role in PG layer formation and that the PG layer alters inflammation around Ti materials.

Graphical Abstract

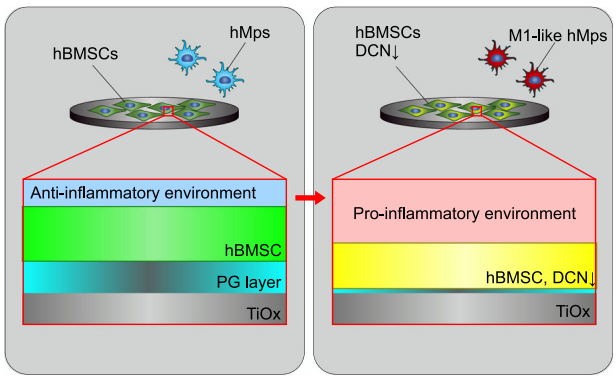

1 Introduction

Dental implants are now widely used to replace missing teeth, with titanium (Ti) is being the material commonly used for dental implants. Osseointegration is an crucial phenomenon for successful implant treatment and is defined as direct contact between the bone and implant without intervening soft tissue as observed in histological analyses using light microscopy [1]. Several studies on implantology have focused on surface modification or bioactive molecule coating [2–7]. However, the molecular mechanisms underlying osseointegration remain unclear.

✉ Shuhei Tsuchiya
s313095@ed.nagoya-cu.ac.jp

[1] Department of Dental Anesthesiology, Division of Oral and Maxillofacial Surgery and Oral Medicine, Hiroshima University Hospital, Hiroshima city, Hiroshima, Japan

[2] Department of Oral and Maxillofacial Surgery, Nagoya City University Graduate School of Medical Sciences, Nagoya, Aichi, Japan

[3] Department of Oral Anatomy, School of Dentistry, Aichi Gakuin University, Nagoya, Aichi, Japan

[4] Institutes of Innovation for Future Society, Nagoya University, Nagoya, Aichi, Japan

Published online: 07 January 2025

Table 1 List of shRNA plasmids

Gene	TRC clone ID	Target sequence
DCN	TRCN0000058553	GCCTCATTTGAATGTGTGAAT
DCN	TRCN0000058554	CGACTTTATCTGTCCAAGAAT
DCN	TRCN0000058555	GCCATTCAACTCGGAAACTAT
DCN	TRCN0000058556	CCGTTTCAACAGAGAGGCTTA
DCN	TRCN0000058557	CCAGGTTGTCTACCTTCATAA
Control	TRC1/1.5	CCGGCAACAAGATGAAGAGCACCAACTCGAGTTGGTGCTCTTCATCTTGTTGTTTTT

It has been reported that a proteoglycan (PG)-rich layer exists at the interface between living bone and Ti oxides (TiOx), covering the surface of Ti implants as observed by transmission electron microscopy (TEM) [8]. Previous studies proposed a molecular model of the PG layer on TiOx hypothesized that dermatan sulfate (DS), glycosylated with decorin (DCN), binds to TiOx directly [9], and DS has indeed been detected at the interface between cultured cells and TiOx in vitro [10, 11]. Researchers have suggested that PG layers play essential roles in both mineralization [10] and immunomodulation of TiOx [12], as implanted Ti has been shown to control inflammation caused by bacterial infection and foreign body reactions after surgical implantation. However, the role of the PG layer during osteogenesis on TiOx remains incompletely elucidated to date.

DCN is one of several structurally related proteoglycans (PGs), classified as small leucine-rich PGs (SLRPs), with a single glycosaminoglycan (GAG) chain consisting of chondroitin sulfate (CS) or dermatan sulfate (DS). The structure of DCN is horseshoe-like or arch-shaped, and collagen molecules bind to the inner concave surface [13]. DCN is present mainly in the extracellular matrix and has a core protein of approximately 40 kDa and a chondroitin sulfate/dermatan sulfate glycosaminoglycan chain. DCN is expressed in various tissues and is an important molecule in wound healing [14] and osteogenesis [15] by suppressing tissue fibrosis through inhibition of TGF (Transforming growth factor)-β activity and other regulatory mechanisms [16]. DCN organizes collagen structures and is involved in wounded skin tissue in vivo [17]. Previous studies have suggested that DCN coating on titanium surfaces inhibits the proliferation and function of fibroblasts and improves those of osteoblasts [18, 19], and the presence of substrate-bound DCN has been reported to influence the effect of TGF-β1 [20]. However, exogenous treatment with DCN does not validate the process of osseointegration in previous reports because these reports focused on surface modification to promote osteogenesis on TiOx implants, and irrelevant molecules such as polydopamine intervened between the TiOx and DCN.

Furthermore, DCN also plays an important role in immunomodulation during macrophage differentiation by inhibiting proliferation and protecting macrophages from apoptosis induction [21]. Macrophages are classified into M1 and M2 subtypes based on their activation state. M1 macrophages release pro-inflammatory factors, while M2 macrophages have anti-inflammatory and immunomodulatory properties that are potentially effective against inflammatory diseases and conditions [22]. Furthermore, DCN is a key paracrine factor that induces macrophage polarization via CD44, a master immunoregulator of mesenchymal stem cells derived from umbilical cord blood [23].

In this study, we used RNA interference with shRNA to determine the effect of DCN synthesized by bone marrow-derived mesenchymal stem cells (BMSCs) on osseointegration, and we observed the PG layer using TEM.

2 Materials and methods

2.1 Cell culture

The human MSC cell line UE7T-13 was obtained from the Japanese Collection of Research Biosources (JCRB; Osaka, Japan). The cells were cultured in Dulbecco's modified Eagle's medium (DMEM) containing 10% fetal bovine serum (FBS) (Sigma-Aldrich, Tokyo, Japan) and 1% penicillin-streptomycin (Fujifilm Wako, Osaka, Japan) at 37 °C in a humidified atmosphere with 5% CO_2 atmosphere.

2.2 Fabrication of Ti samples and characterization of surfaces

Pure Ti plates were obtained from Ofa Co., Ltd. (Chiba, Japan), and Ti foil was sourced from Nirako (Tokyo, Japan). A smooth surface was prepared for the experiments, as described in a previous study [12].

2.3 Generation of stable cell lines

MISSION® shRNA (target: DCN) and MISSION® non-mammalian shRNA control plasmids listed in Table 1 were obtained from Sigma-Aldrich Co. LLC (Tokyo, Japan). Five shRNA plasmids and control plasmids were transfected into UE7T-13 cells using ViaFect™ Transfection Reagent (Promega KK, Tokyo, Japan), and 12 independent puromycin-resistant single clones were successfully

Table 2 List of primers

Gene	Sequence 5′-3′	3′-5′	Accession number of reference
DCN	GGAGCTTCACTTGGACAACAAC	GGCAGAAGTCACTTGATCCAAC	NM_133503.3
Col1a1	ATGTGCCACTCTGACTGGAAG	ACCAGTCTCCATGTTGCAGAAG	NM_000088.3
Runx2	CCTTGACCATAACCGTCTTCAC	AAGCTTCTGTCTGTGCCTTC	NM_001024630.3
ALPL	AGCTGAACAGGAACAACGTG	ATTCTGCCTCCTTCCACCAG	NM_000478.5
OCN	AATCCGGACTGTGACGAGTTG	CTGGAGAGGAGCAGAACTGG	NM_199173.5
Acta2	ACCACTATGTACCCTGGCATTG	CGATCCAGACAGAGTATTTGCG	NM_001141945.2
FN1	AAGCAAGCCCGGTTGTTATG	AAACCAACGCATTGCCTAGG	NM_054034.2
TGF-β1	TGACCTGGCCACCATTCATG	CGTGGAGCTGAAGCAATAGTTG	NM_000660.7
IL-6	AATGAGGAGACTTGCCTGGTG	TGTACTCATCTGCACAGCTCTG	NM_000600.4
IL-10	ATCAAGGCGCATGTGAACTC	AAGGCATTCTTCACCTGCTC	NM_000572.3
IDO	TCCTTACTGCCAACTCTCCAAG	CGTCCATGTTCTCATAAGTCAGG	NM_002164.5
CD80	GTTATCCACGTGACCAAGGAAG	TTGTGCCAGCTCTTCAACAG	NM_005191.4
CD86	ACTGTACGACGTTTCCATCAGC	AGCCGCGTCTTGTCAGTTTC	NM_001206924.1
CD163	AAGACGCTGCAGTGAATTGC	AATGGCCAACAGAACAACCC	NM_001370145.1
CD206	TGGAGCAGGTGGAAGATCTATG	ACTTGAACGGGAATGCACAG	NM_002438.3
GAPDH	AGCAAGAGCACAAGAGGAAGAG	TCTACATGGCAACTGTGAGGAG	NM_001289745.2

Runx2 runt-related transcription factor 2, *ALPL* alkaline phosphatase, *OCN* osteocalcin, *Acta2* actin alpha 2, *FN1* fibronectin 1, *IDO* indoleamine 2,3-dioxygenase 1, *GAPDH* glyceraldehyde-3-phosphate dehydrogenase

established. These methods have been detailed in a previous study [12]. The depletion efficiency was determined by real-time RT-PCR and western blot analysis. The most effective shRNA was chosen to deplete DCN for the remainder of the study (sh-BMSCs). Non-target control cells were transfected using the same method (N-BMSCs).

2.4 Real-time PCR

Cells were seeded on Ti plates at a density of $5 \times 10^2/cm^2$ and cultured for 7 and 14 days. Total RNA was isolated using TRIzol® LS Reagent (Thermo Fisher Scientific, Waltham, MA, USA), and cDNA was synthesized using ReverTra Ace™ qPCR RT Master Mix and gDNA Remover (Toyobo Co., Ltd., Osaka, Japan) according to the manufacturer's protocol. Quantitative real-time RT-PCR was performed using THUNDERBIRD™ SYBR® qPCR Mix (Toyobo) and an Mx3000P™ Real-Time qPCR System (Agilent Technologies International Japan, Ltd., Tokyo, Japan). The expression of target transcripts was normalized against the expression of glyceraldehyde-3-phosphate dehydrogenase (GAPDH), and relative changes in gene expression were determined using the $2^{-\Delta\Delta Ct}$ method. The primers used in this study are listed in Table 2.

2.5 Western blotting

Cell lysis and protein extraction were performed using RIPA buffer (Thermo Fisher Scientific Inc., Tokyo, Japan). Samples were separated by SDS-PAGE and transferred onto a PVDF membrane. After blocking with 5% nonfat dry milk (Cell Signaling Technology, Tokyo, Japan) or 2% bovine serum albumin (Nacalai Tesque, Inc., Tokyo, Japan) in Tween-PBS, each membrane was incubated with the following primary antibodies: anti-GAPDH; 1:10,000; ab181602; Abcam, Cambridge, United Kingdom, anti-DCN; 1:1000; sc-73896; Santa Cruz Biotechnology, Inc., Heidelberg, Germany, anti-BGN; 1:1000; sc-100857; Santa Cruz Biotechnology, Inc., anti-TGFβ1; 1:1000; sc-130348; Santa Cruz Biotechnology, Inc., anti-vinculin; 1:10,000; ab129002; Abcam, or anti-RhoA; 1:5000; #2117; Cell Signaling Technology, Inc. for 12 h at 4 °C. The membrane was then incubated with anti-rabbit IgG horseradish peroxidase-linked whole antibody (from donkey) (1:10,000, NA934V; GE Healthcare, Tokyo, Japan) or anti-mouse IgG HRP peroxidase-linked whole antibody (1:10,000, NXA931V, GE Healthcare), as the secondary antibody for 1 h at room temperature. Antibody reactions were detected using ECL™ Prime Western Blotting Reagent (GE Healthcare) or ECL Select Western Blotting Reagent (GE Healthcare) and a LuminoGraph I system (ATTO Corp., Tokyo, Japan).

2.6 Flow cytometry

Cells were suspended in stain buffer (FBS) (BD Biosciences, San Jose, CA, USA) and incubated with CD (cluster of differentiation) 14-PE-Cy7 (Clone 61D3), CD19-

PE-Cy7 (Clone SN6), CD34-PE-Cy7 (Clone 4H11), CD45-PE-Cy7 (Clone HI30), CD73-APC (Clone AD2), CD90-APC (Clone 5E10), CD105-PE-Cy7 (Clone SN6), and HLA-DR-Alexa Fluor 700 (Clone LN3) for 30 min on ice. All antibodies were purchased from Thermo Fisher Scientific. The stained cells were analyzed using a FACSCanto™ II system (Becton, Dickinson and Company, Tokyo, Japan).

2.7 Cell proliferation assay

Ti foil was punched out to make thin circular plates (6 mm in diameter), then placed in 96-well plates. After seeding 1×10^2 cells on the Ti plates for 1, 2, 3, 7, and 14 days, proliferation assays were performed using the Cell Counting Kit-8 (Dojindo Laboratories, Kumamoto, Japan) following the manufacturer's instructions. Absorbance was determined using an Infinite 200 PRO system and i-control software (Tecan Japan Co. Ltd., Kanagawa, Japan).

2.8 Initial cell adhesion assay

To assay initial cell adhesion, 1×10^4 cells were seeded onto Ti plates (15 mm in diameter) and cultured for 1, 2, or 3 h in DMEM. Each plate was fixed with 10% formalin and stained with 0.5% crystal violet (Fujifilm Wako, Osaka, Japan) for 10 min at room temperature. After washing with distilled water several times to remove the excess solution, the dye was eluted with 10% acetic acid (Fujifilm Wako), and the absorbance was measured at 540 nm.

2.9 Alizarin red S staining

Cells were seeded on Ti plates (15 mm in diameter) at a density of $5 \times 10^2/cm^2$ and cultured for 14 days in DMEM. The medium was changed to osteoinduction medium (DMEM supplemented with 50 µg/mL ascorbic acid, 100 nM dexamethasone, and 10 mM β-glycerophosphate), and the cells were cultured for another 14 days. Each plate was fixed with 10% formalin and stained with 1% alizarin red S solution (Fujifilm Wako, Osaka, Japan) for 30 min at room temperature. After staining, the cells were washed several times with distilled water to remove excess solution. Quantification was performed according to a previous report [24], and absorbance was measured at 405 nm.

2.10 Immunocytochemical (ICC) analysis

Cells were seeded on Ti plates (15 mm in diameter) at a density of $5 \times 10^2/cm^2$ and cultured for 24 h. The cells were fixed with 4% paraformaldehyde for 15 min at room temperature and permeabilized with 0.2% Triton X-100 in PBS for 20 min. After blocking using Blocking One Histo (Nacalai Tesque, Inc., Kyoto, Japan) for 10 min, each plate was incubated with anti-vinculin (1:250; ab129002; Abcam) for 14 h at 4 °C, then incubated with goat anti-Rabbit IgG (H+L) highly cross-adsorbed secondary antibody, Alexa Fluor 546 (4 µg/mL; A11035; Thermo Fisher Scientific) for 1 h and Acti-stain™ 488 phalloidin (100 nM, Cytoskeleton, Inc. Co., Denver, CO, USA) for 1 h in the dark. Finally, each plate was mounted with DAPI (Vector Laboratories, Inc., Burlingame, CA, USA) and observed using a BZ-X810 All-in-One Fluorescence Microscope (Keyence, Osaka, Japan). Ten fields of view were randomly photographed and cells that were not in contact with the outer frame or each other were analyzed. Image analysis was performed using ImageJ software. Images of vinculin staining were thresholded to identify the adhesion complexes.

2.11 Transmission electron microscopy

Cells were seeded on Ti foil (6 mm in diameter) at a density of $5 \times 10^2/cm^2$. After 14 days of cultivation, the samples were stained with 0.05% ruthenium red solution for 1 h between pre- and post-fixation. After embedding in EPON resin, the foil was physically removed, and the samples were re-embedded in EPON resin. These methods have been described in detail in a previous study [12]. The samples were sectioned using an ultramicrotome (EM UC7i, Leica, Tokyo, Japan), stained with lead citrate for 5 s, and observed under a transmission electron microscope (JEM-1400PLUS, JEOL).

2.12 Immunotolerance assay of BMSCs and human macrophages

Immunotolerance assays were performed as described previously [12]. Total RNA was extracted to analyze macrophage polarization. Furthermore, protein expression levels of IL-6 and IL-10 in the supernatant were quantified using enzyme-linked immunosorbent assay (ELISA) (Proteintech, Tokyo, Japan) according to the product instructions.

2.13 Decellularization assay

Cells were seeded on Ti plates at a density of $5 \times 10^2/cm^2$ and cultured for 14 days. Each plate was then frozen in PBS for decellularization. Thawed plates were washed three times with PBS to prepare N-BMSC-decellularized surfaces (N-Ti) and sh-BMSC-decellularized surfaces (sh-Ti). Fresh N- and sh-BMSCs were seeded onto the plates at a density of $5 \times 10^2/cm^2$. After 14 days of cultivation, total RNA was extracted to evaluate gene expression.

2.14 Image and statistical analyses

Image analysis was carried out using ImageJ software (https://imagej.net/Welcome; National Institutes of

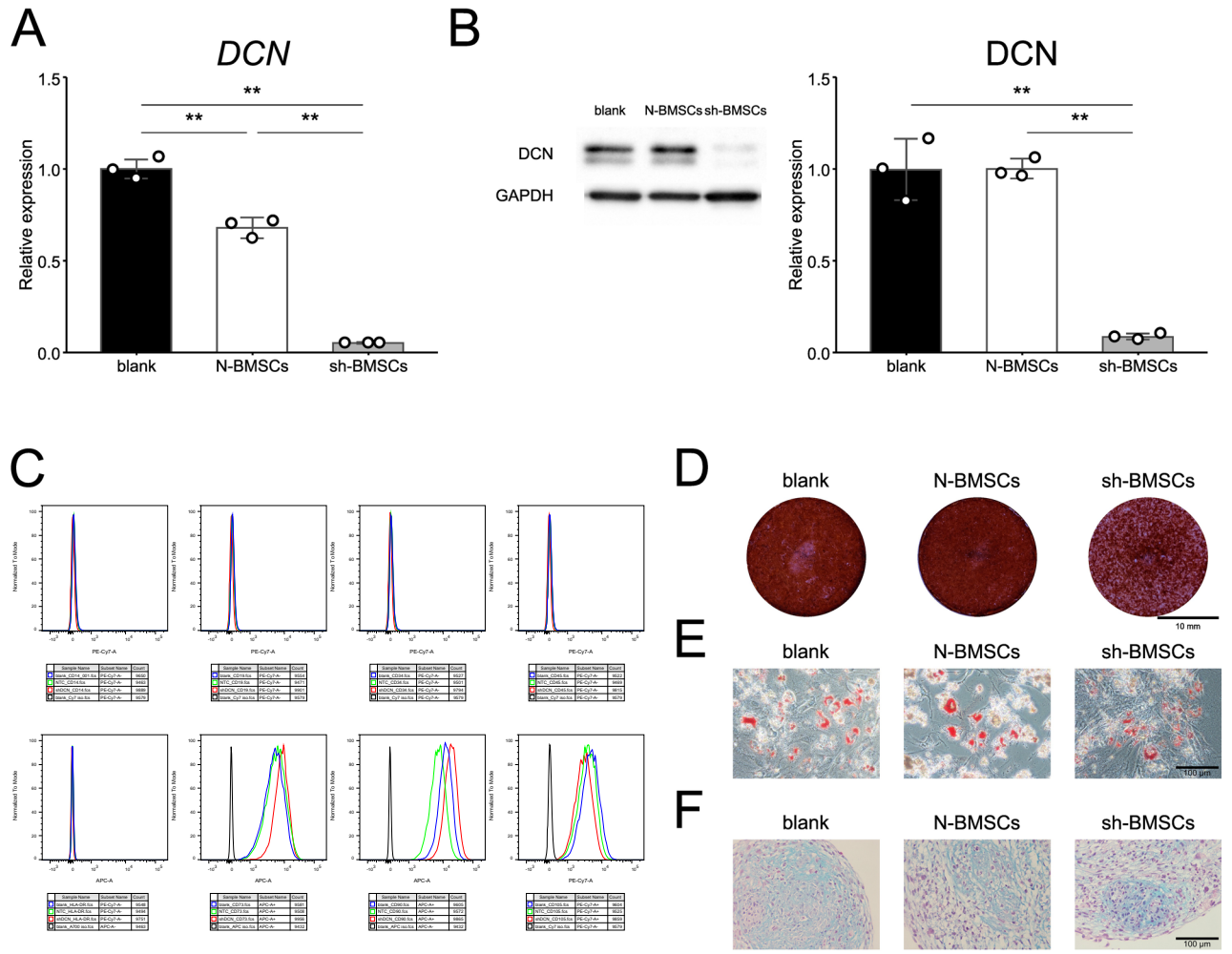

Fig. 1 Characterization of N-BMSCs and sh-BMSCs. **A** mRNA and **B** protein expression analysis of DCN. **C** Representative flow cytometry analysis of cell surface markers. **D** Alizarin red S staining, **E** Oil Red O staining, and **F** Alcian blue staining after osteogenic induction, adipogenic induction, and chondrogenic induction culture. $^{**}p < 0.01$

Health, Bethesda, MD, USA). All experiments were carried out in triplicate, and the data are presented as means ± standard deviation. The statistical analysis was performed using R software (http://www.R-project.org; Vienna, Austria), and significance was analyzed using Welch's t-test or one-way ANOVA with Tukey's multiple comparison test. Results with $p < 0.05$ were considered statistically significant.

3 Results

3.1 Characterization of N-BMSCs and sh-BMSCs

DCN gene expression was significantly decreased to approximately 68% in N-BMSCs and 5.0% in sh-BMSCs compared to blank (no vector was transfected) BMSCs (Fig. 1A). The protein expression of DCN in sh-BMSCs was significantly decreased to approximately 8.5% compared to that in blank- and N-BMSCs (Fig. 1B). Flow cytometry and multipotency assessments of blank, N-, and sh-BMSCs were performed according to the minimal criteria proposed by the International Society for Cellular Therapy [25]. The expression levels of CD14, CD19, CD34, CD45, and HLA-DR were less than 2%, and those of CD73, CD90, and CD105 were greater than 95% in all cell groups (Fig. 1C). All experimental groups had the capacity for osteogenic (Fig. 1D), adipogenic (Fig. 1E), and chondrogenic differentiation (Fig. 1F).

3.2 Effect of DCN on PG layer formation

To evaluate the effect of DCN on the PG layer formation on the surface of TiOx, ultrastructural observations by TEM imaging were performed. After 14 days of cultivation on TiOx, an area stained with ruthenium red was observed between the cell membrane and TiOx in N-BMSCs; however, this stained area was not observed in sh-BMSCs (Fig. 2A).

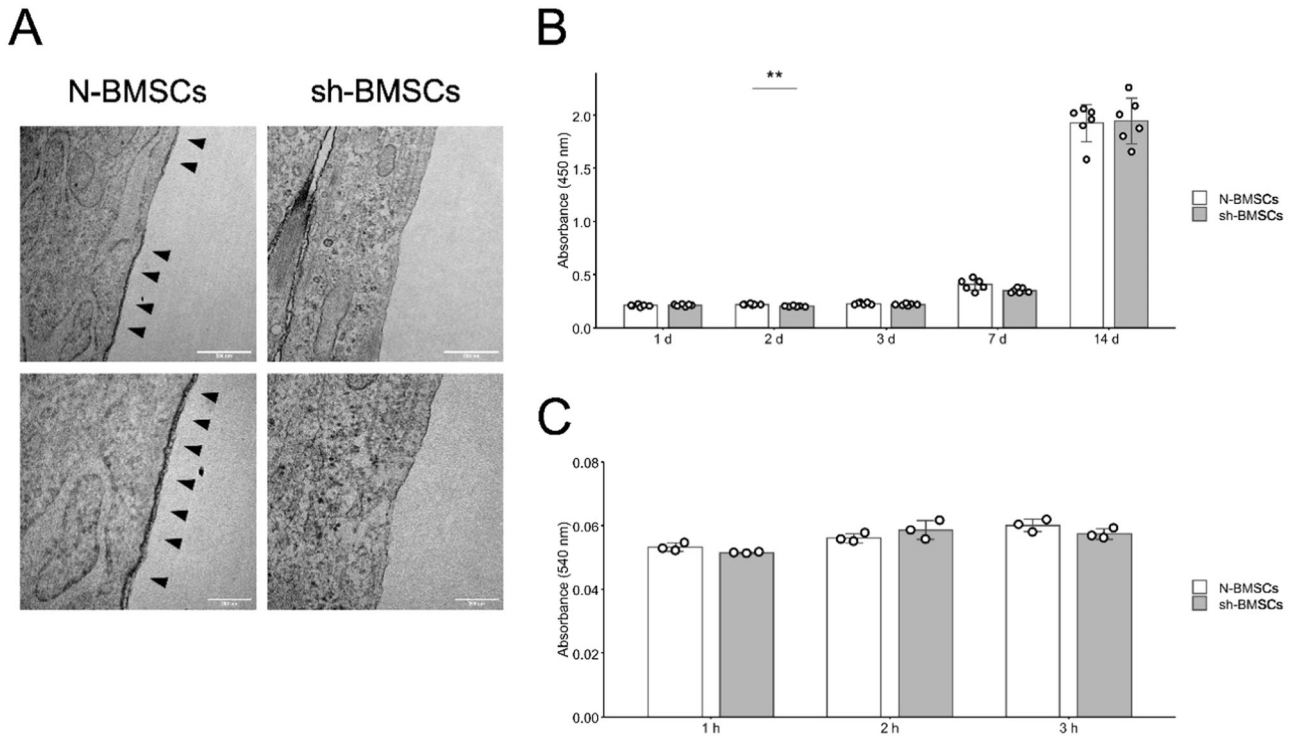

Fig. 2 **A** Transmission electron micrograph of the cell–TiOx interface. The ruthenium-positive areas were detected at 14 days of N-BMSC cultivation (arrowheads). **B** Proliferation of N-BMSCs and sh-BMSCs on TiOx on days 1, 2, 3, 7, and 14. **C** Initial cell adhesion of N-BMSCs and sh-BMSCs to TiOx at 1, 2, and 3 h. This figure is representative of three independent experiments. $^{**}p < 0.01$

3.3 Effects of DCN on cell proliferation and initial cell adhesion

A CCK-8 assay was performed to evaluate the effect of DCN on cell proliferation on TiOx. At 48 h of cultivation, the number of sh-BMSCs was significantly lower than that of N-BMSCs. However, there was no significant difference at any other time point (Fig. 2B). The initial cell attachment was not significantly different between N-BMSCs and sh-BMSCs (Fig. 2C).

3.4 Effect of DCN on cell extension

The morphology of the cells that adhered to TiOx after 24 h of cultivation was visualized by immunofluorescence staining (Fig. 3A, green: F-actin, red: vinculin, blue: DAPI). The dot plots show the individual values of the area (Fig. 3B), major (Fig. 3C), minor (Fig. 3D), aspect ratio (Fig. 3E), Feret diameter (Fig. 3F), and minimum Feret diameter (Fig. 3G) measured using ImageJ software. The area and the minor and minimum Feret diameters of sh-BMSCs were significantly smaller than those of N-BMSCs, while the aspect ratio of sh-BMSCs was considerably higher than that of N-BMSCs.

3.5 Effect of DCN on osteogenic properties

RT-qPCR was performed to evaluate the silencing of DCN and its effects on osteogenesis-related genes after 7 and 14 days of cultivation on TiOx (Fig. 4A–E). The mRNA expression in sh-BMSCs was significantly lower than that in N-BMSCs with no expression of OCN at day 14. Calcified nodules formed in N- and sh-BMSCs after 14 days of cultivation and 14 days of osteogenic induction (Fig. 4F), and quantification showed that the absorbance of sh-BMSCs was significantly lower than that of N-BMSCs (Fig. 4G).

3.6 Effect of DCN on fibrotic markers and extracellular matrix

The expression of fibrosis-related genes was analyzed using RT-qPCR (Fig. 5A–C). All fibrosis-related gene expressions of sh-BMSCs were significantly lower than those of N-BMSCs, except for FN1, on day 14.

The expression of proteins related to the extracellular matrix was analyzed by western blotting (Fig. 5D). Quantitative analysis showed that the expression of BGN in sh-BMSCs was significantly lower than that in N-BMSCs (Fig. 5E); however, there was no significant difference in the expression of TGF-β1 (Fig. 5F), vinculin (Fig. 5G), and RhoA (Fig. 5H).

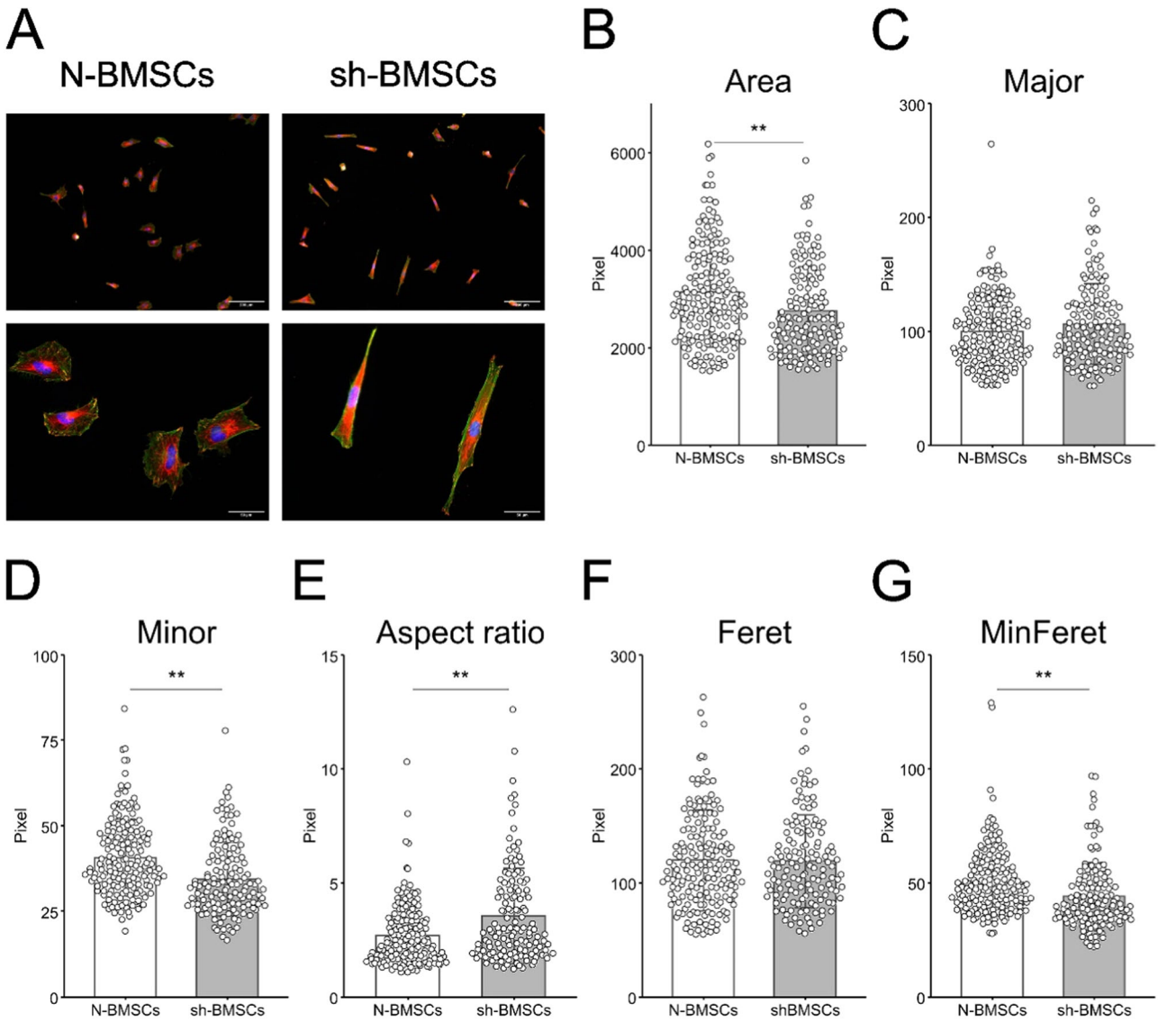

Fig. 3 Immunofluorescence staining analysis of N-BMSCs and sh-BMSCs after 24 h of cultivation on TiOx. **A** Expression of vinculin. Green: F-actin, Red: vinculin, Blue: DAPI. **B** Area, **C** major, **D** minor, **E** aspect ratio, **F** Feret, and **G** minimum Feret were measured to evaluate cell adhesion and extension. $^{**}p < 0.01$

3.7 Effect of DCN on immunotolerance

RT-qPCR was performed to analyze the effect of DCN on the immunotolerance of BMSCs to TiOx. The expression levels of IL-6 and IL-10 in sh-BMSCs were significantly lower than in N-BMSCs (Fig. 6A, B). However, there was no significant difference in IDO expression between N- and sh-BMSCs (Fig. 6C). CM derived from N- and sh-BMSCs cultured on TiOx affected the differentiation of human macrophages (hMps). The expression of IL-6 and IDO, markers of M1 Mps, was significantly higher in hMps treated with CM derived from sh-BMSCs than in those treated with CM derived from N-BMSCs (Fig. 6D, F). The expression of CD206, a marker of M2 Mps, was significantly higher in hMps treated with CM derived from sh-BMSCs than in those treated with CM derived from N-BMSCs (Fig. 6J). ELISA quantified the protein expression levels of IL-6 and IL-10 in the supernatant. Both protein expressions in the culture supernatant of BMSCs cultured on TiOx (Fig. 6K, L) and after stimulating hMps (Fig. 6M, N) showed the same tendency as the RT-qPCR results.

3.8 Effect of PG layer on gene expression in BMSCs

A decellularisation assay was performed to analyze the effects of the PG layer. The expression levels of *Col1a1*, *Runx2*, *OCN*, and *TGF-β1* in sh-BMSCs were significantly lower than those in N-BMSCs on both N-Ti and sh-Ti (Fig. 7A, B, D, G). The expression levels of *ALPL* and *Acta2* in sh-BMSCs were significantly lower than those in TNC-BMSCs

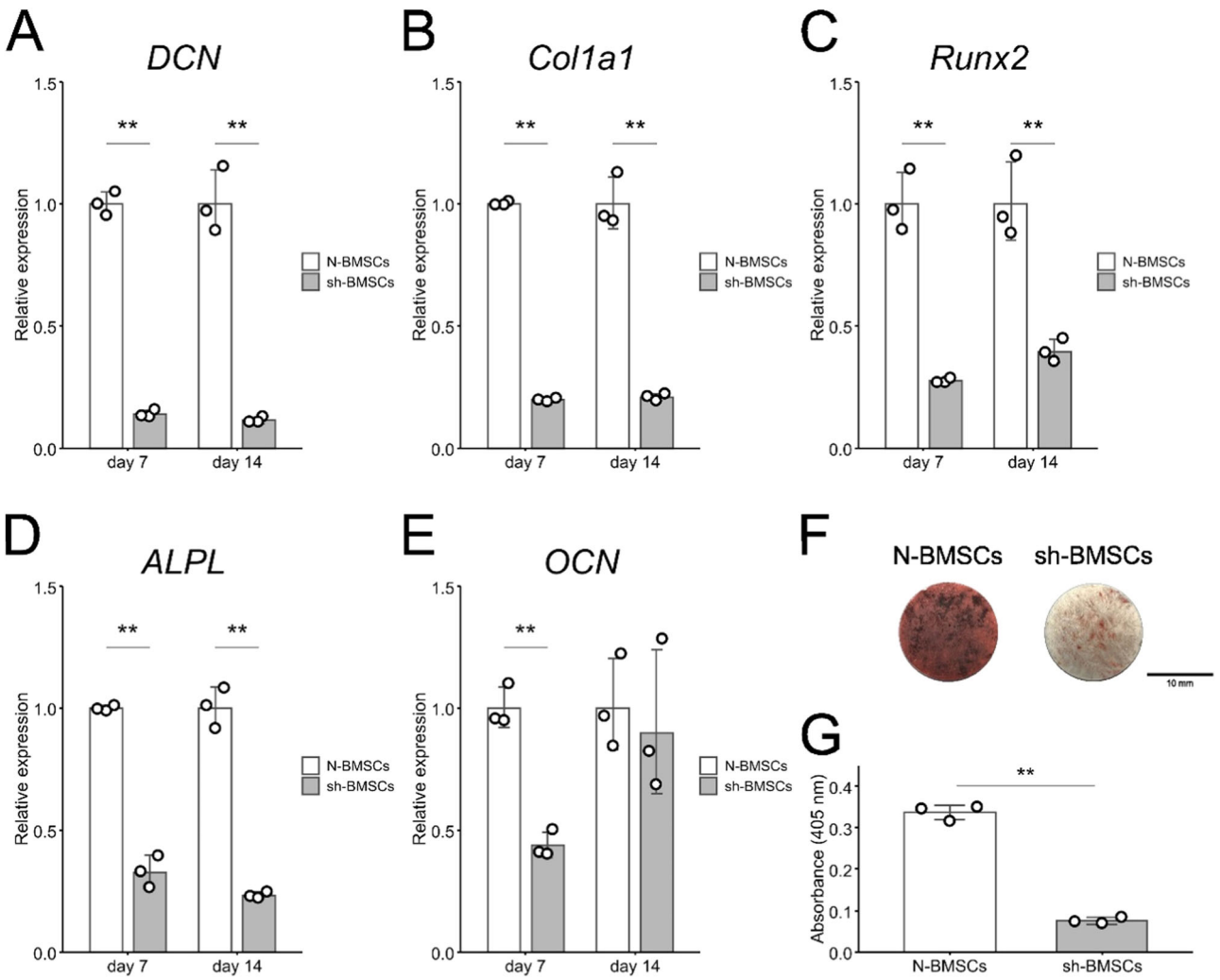

Fig. 4 Osteogenic capacity of N-BMSCs and sh-BMSCs. Gene expression of **A** *DCN*, **B** *Col1a1*, **C** *Runx2*, **D** *ALPL*, and **E** *OCN* after 7 and 14 days of cultivation on TiOx. Mineralized nodule formation by alizarin red S staining (**F**) and quantitative analysis (**G**). This figure is representative of three independent experiments. $^{**}p < 0.01$

on sh-Ti; however, there was no significant effect on N-Ti (Fig. 7C, E). Regarding FN1, there was no significance between N-BMSCs and sh-BMSCs on either N-Ti or sh-Ti (Fig. 7F). SEM-EDX analysis did not detect elemental sulfur on the N-Ti (Fig. 7H) and blank Ti (Fig. 7I).

4 Discussion

In this study, we investigated whether DCN affects BMSCs on TiOx using long-term RNA interference. Flow cytometry and multipotency assays showed that the osteogenic and chondrogenic capacities of sh-BMSCs were consistent with those reported previously [26]. In contrast, DCN in BMSCs did not affect cell surface markers of CD. These results suggest that assaying multipotency was relevant to the maintenance of stemness in BMSCs compared to the CD marker assay.

TEM analysis showed that the PG layer on TiOx formed by BMSCs depleted of DCN was decreased compared to that formed by BMSCs depleted of chondroitin-4-sulfotransferase-1 [12]. These results suggest that DCN is the main component of the PG layer on TiOx. These results suggest that other molecules or a small amount of DCN played an important role in the adherence between BMSCs and TiOx because sh-BMSCs did not detach from TiOx for two weeks. The electron-dense layer between adjacent sh-BMSCs may contain other proteoglycans involved in cell-cell adhesion, such as syndecans. A different approach is needed to clarify this because ruthenium red usually stains whole proteoglycans.

DCN did not affect cell proliferation or initial adhesion to TiOx. Wang et al. reported that the knockdown of DCN in human chondrocytes suppressed cell proliferation and adhesion [27], while Mochida et al. reported that DCN in MC3T3-E1 cells did not affect cell proliferation [28]. In

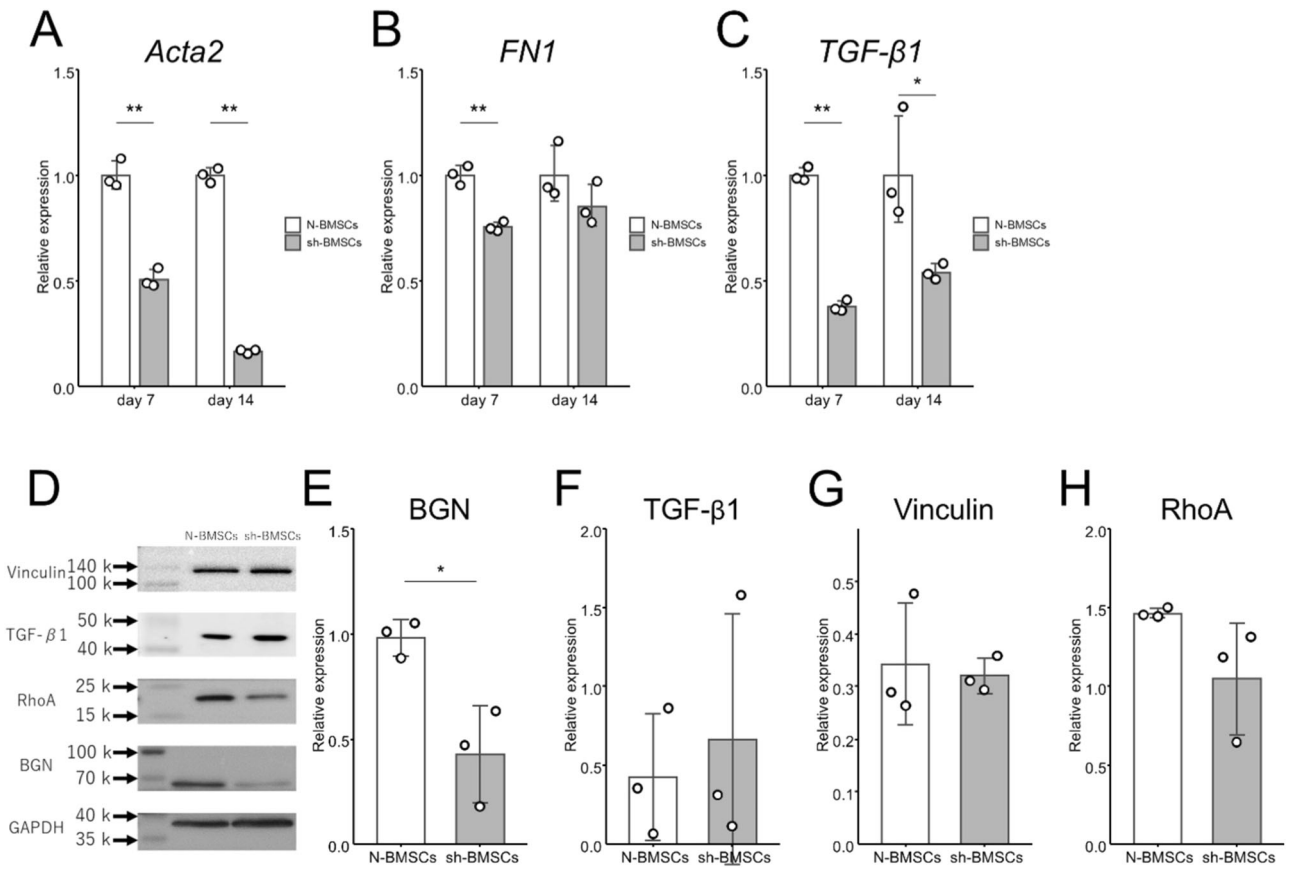

Fig. 5 Gene expression of **A** *Acta2*, **B** *FN1*, and **C** *TGF-β1* after 7 and 14 days of cultivation on TiOx. Western blotting analysis of extracellular matrix after 14 days of cultivation on TiOx (**D**) and semi-quantification (**E**–**H**). This figure is representative of two independent experiments. *p < 0.05, **p < 0.01

contrast, MC3T3-E1 cell proliferation was affected by the amount of exogenous DCN [19], and the proliferation of human fibroblasts on TiOx was attenuated depending on the amount of exogenous DCN [29]. These differences were due to the cell type and culture substrate (TiOx versus polystyrene), and endogenous and exogenous DCN affected cell proliferation and attachment. In this study, we focused on the osteogenesis of TiOx during osseointegration, which is suitable for analyzing the actual process of osseointegration in vitro.

DCN inhibited the extension of BMSCs in the minor axis direction without differences in vinculin expression between N- and sh-BMSCs. Cells grown on PG matrices are altered during processes involved in normal cell adhesion via vinculin clustering [30]. Previous reports have shown that DCN is important in maintaining collagen structure [31] and regulating fibril assembly [32]. From the above, depletion of DCN caused a disturbance of the collagen structure, thereby affecting the cell morphology on TiOx because collagen is one of the key factors in cell attachment on TiOx [33]. In the future, the ultramicrostructure of collagen on TiOx should be observed using TEM to analyze the function of DCN on TiOx.

Previous reports have shown that DCN may act as an inhibitor of collagen matrix mineralization on a polystyrene substrate [28]. However, the osteogenic capacities of osteoblasts on TiOx coated with exogenous DCN improved [19]. The expression of fibrotic markers in this study was consistent with that in a previous report [19]. DCN connects TGF-β and suppresses the osteogenic capacities through the Smad pathway [34, 35]. It was suggested that the discrepancy in the osteogenic properties of DCN derived from cells on polystyrene and TiOx was caused by different pathways on the TiOx and polystyrene substrates. In addition, the mineralization on TiOx was caused by a different mechanism from collagen fiber mineralization because collagen fibers were not observed in the PG layer by N- and sh-BMSCs on TiOx at any time point in the TEM analysis. Furthermore, the difference in osteogenic properties was caused by the cell type because MC3T3 cells are characterized by an osteoblastic phenotype and are different from the MSCs used in this study.

DCN on TiOx altered immunomodulation in MSC. Secreted inflammatory cytokines affect macrophage polarization toward the anti-inflammatory phenotype. The differences in IL-6 and IL-10 expression between BMSC-depleted DCN and control BMSCs were greater than that

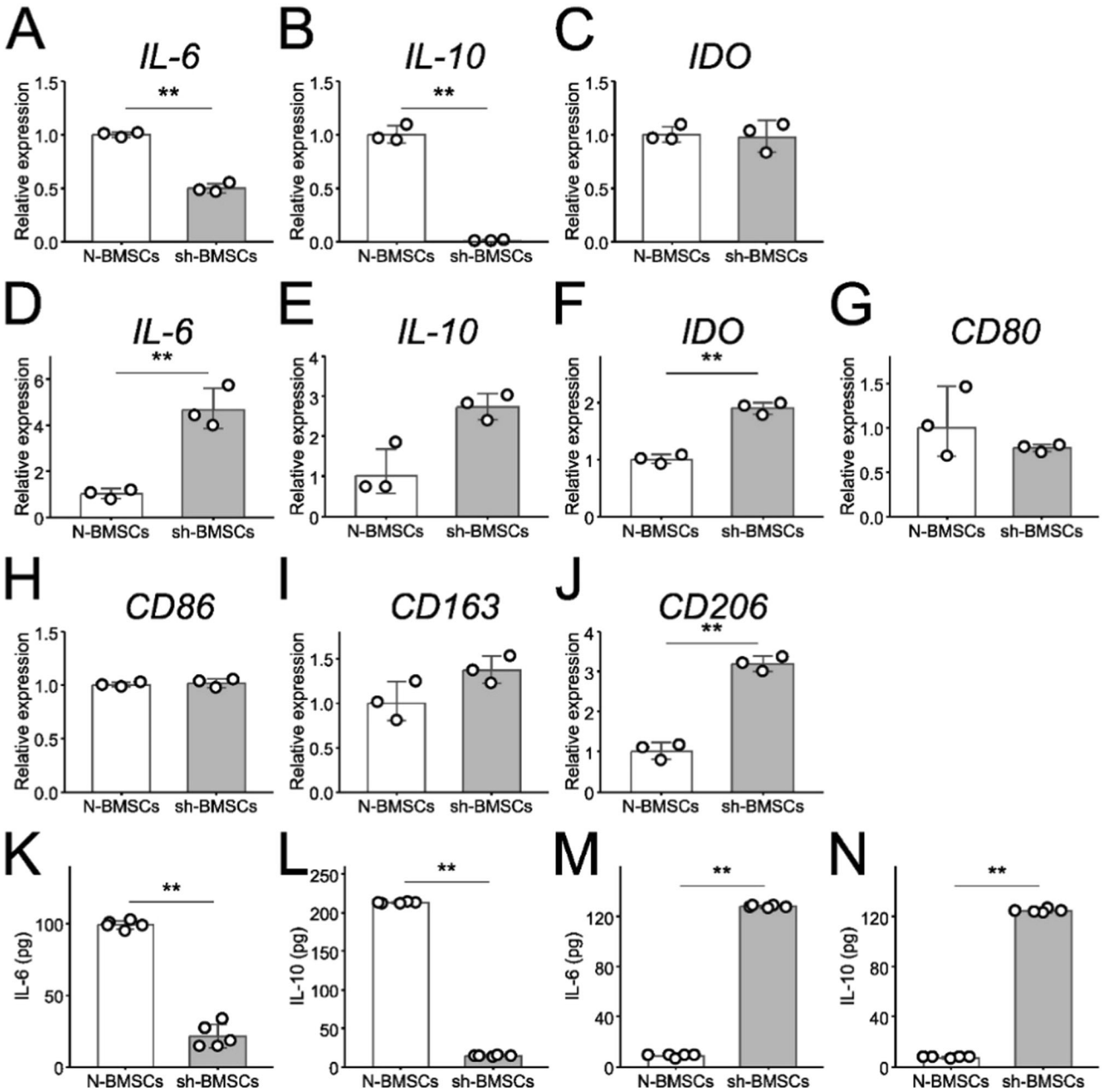

Fig. 6 Gene expression related to immunotolerance in N-BMSCs and sh-BMSCs after 14 days of TiOx (**A**–**C**) cultivation and in CM-treated hMps derived from N-BMSCs and sh-BMSCs (**D**–**J**). Protein expression levels of IL-6 and IL-10 in the supernatant of BMSCs cultured on TiOx (**K**, **L**) and after stimulating hMps (**M**, **N**). $^{**}p < 0.01$

between C4ST-1-depleted BMSCs and control BMSCs. The difference in the PG layer area between BMSC-depleted DCN and control BMSCs was greater than the difference between C4ST-1-depleted BMSCs and control BMSCs [12]. Accumulating evidence has shown that DCN regulates the bioactivities of cell growth factors and participates in ECM assembly because DCN acts as a ligand for various cytokines and growth factors by direct or indirect interactions [36]. Combining the TEM observations and gene expression data related to immune tolerance suggested that the PG layer on TiOx controlled the immunomodulatory capacity of BMSCs on TiOx.

IL-10 is a well-known anti-inflammatory mediator [37]. It has been suggested that sh-BMSCs establish a pro-inflammatory environment next to TiOx, given that the expression of IL-10 in sh-BMSCs was much lower than in N-BMSCs. Furthermore, the polarization of hMps shifted to M1-like Mps, which agrees with our previous study [12]. Taken together, the PG layer possibly establishes an anti-inflammatory environment around the TiOx materials.

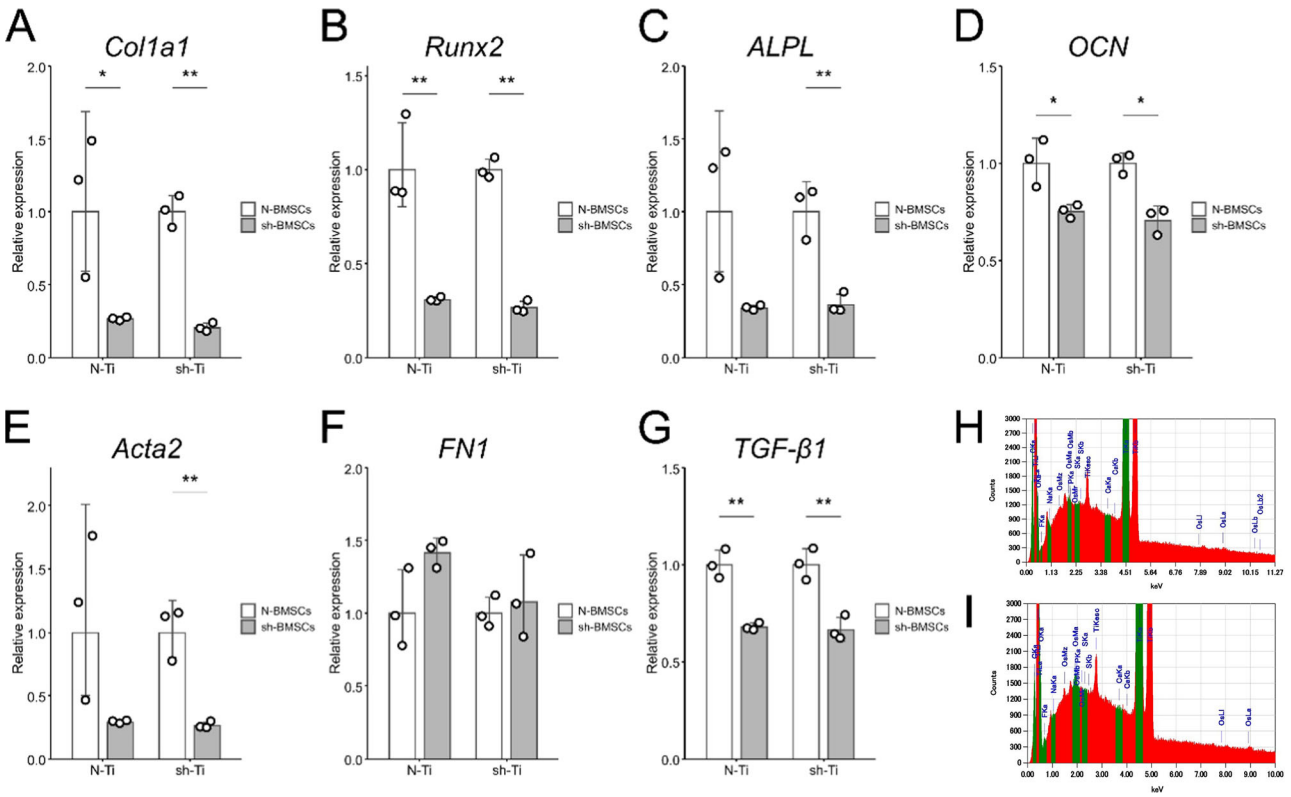

Fig. 7 Decellularization assay analysis of N-BMSCs and sh-BMSCs. Gene expression of **A** *Col1a1*, **B** *Runx2*, **C** *ALPL*, **D** *OCN*, **E** *Acta2*, **F** *FN1*, and **G** *TGF-β1* after 14 days of cultivation on decellularized TiOx. SEM-EDX analysis of decellularized Ti surfaces (**H**, **I**). This figure is representative of two independent experiments. *$p < 0.05$, **$p < 0.01$

Further analysis of the immunotolerance using various surfaces would support clinical applications.

The decellularization assay revealed few differences between N- and sh-Ti, and SEM-EDX did not detect sulfur on either surface. Although we tried to prepare a decellularized surface to investigate the influence of endogenous and exogenous DCN, the decellularization of TiOx was difficult. The possible reasons are as follows: long-term cultivation led to several layers of cells, and the cells next to the TiOx became undernourished, or the interfacial strength between the cells and the TiOx was not strong under in vitro conditions. The ECM may have peeled off from the TiOx surface when the cells were thawed. Therefore, verifying the effects of DCN depletion in vivo is necessary.

From this study, endogenous DCN was suggested to have important roles in osseointegration. Because it is difficult to harvest bone tissue adjacent to osseointegrated titanium implants, creating a system for preoperative evaluation is important. For example, blood tests or sampling of bone tissue at the time of implant placement for gene expression tests can be used in clinical practice. Furthermore, the method we used in this study can be applied to other target genes. Further research is required to provide reliable implant treatment.

5 Conclusions

DCN in BMSCs on TiOx was the main component of the PG layer. In addition, DCN affected the osteogenesis and immunomodulation of BMSCs on TiOx.

Author contributions The authors confirm their contributions to the paper are as follows: study conception and design: Shuhei Tsuchiya and Kazuto Okabe; data collection: Hisanobu Kamio; analysis and interpretation of results: Hisanobu Kamio; draft manuscript preparation: Shuhei Tsuchiya and Hisanobu Kamio. All the authors reviewed the results and approved the final version of the manuscript.

Funding This work was supported in part by grants from the Japanese Ministry of Education, Culture, Sports, Science, and Technology (Kakenhi Kiban C, 21K09955 to Shuhei Tsuchiya and Kakenhi Kiban C, 19K10264 to KO, Kakenhi Wakate, 22K17091 to HK) and the Terumo Life Science Foundation.

Compliance with ethical standards

Conflict of interest The authors declare no competing interests.

Publisher's note Springer Nature remains neutral with regard to jurisdictional claims in published maps and institutional affiliations.

Open Access This article is licensed under a Creative Commons Attribution-NonCommercial-NoDerivatives 4.0 International License, which permits any non-commercial use, sharing, distribution and reproduction in any medium or format, as long as you give appropriate credit to the original author(s) and the source, provide a link to the Creative Commons licence, and indicate if you modified the licensed material. You do not have permission under this licence to share adapted material derived from this article or parts of it. The images or other third party material in this article are included in the article's Creative Commons licence, unless indicated otherwise in a credit line to the material. If material is not included in the article's Creative Commons licence and your intended use is not permitted by statutory regulation or exceeds the permitted use, you will need to obtain permission directly from the copyright holder. To view a copy of this licence, visit http://creativecommons.org/licenses/by-nc-nd/4.0/.

References

1. Albrektsson T, Johansson C. Osteoinduction, osteoconduction and osseointegration. Eur Spine J. 2001;10(Suppl 2):S96–101. https://doi.org/10.1007/s005860100282
2. Huang J, Zhang X, Yan W, Chen Z, Shuai X, Wang A, et al. Nanotubular topography enhances the bioactivity of titanium implants. Nanomedicine. 2017;13:1913–23. https://doi.org/10.1016/j.nano.2017.03.017
3. Kopf BS, Schipanski A, Rottmar M, Berner S, Maniura-Weber K. Enhanced differentiation of human osteoblasts on Ti surfaces pretreated with human whole blood. Acta Biomater. 2015;19:180–90. https://doi.org/10.1016/j.actbio.2015.03.022
4. Sverzut AT, Crippa GE, Morra M, de Oliveira PT, Beloti MM, Rosa AL. Effects of type I collagen coating on titanium osseointegration: histomorphometric, cellular and molecular analyses. Biomed Mater. 2012;7:035007. https://doi.org/10.1088/1748-6041/7/3/035007
5. Jiang J, Wan F, Yang J, Hao W, Wang Y, Yao J, et al. Enhancement of osseointegration of polyethylene terephthalate artificial ligament by coating of silk fibroin and depositing of hydroxyapatite. Int J Nanomedicine. 2014;9:4569–80. https://doi.org/10.2147/IJN.S69137
6. Shen X, Ma P, Hu Y, Xu G, Zhou J, Cai K. Mesenchymal stem cell growth behavior on micro/nano hierarchical surfaces of titanium substrates. Colloids Surf B Biointerfaces. 2015;127:221–32. https://doi.org/10.1016/j.colsurfb.2015.01.048
7. Camargo WA, Takemoto S, Hoekstra JW, Leeuwenburgh S, Jansen JA, van den Beucken J, et al. Effect of surface alkali-based treatment of titanium implants on ability to promote in vitro mineralization and in vivo bone formation. Acta Biomater. 2017;57:511–23. https://doi.org/10.1016/j.actbio.2017.05.016
8. Ayukawa Y, Takeshita F, Inoue T, Yoshinari M, Ohtsuka Y, Murai K, et al. An ultrastructural study of the bone-titanium interface using pure titanium-coated plastic and pure titanium rod implants. Acta Histochem Cytochem. 1996;29:243–54. https://doi.org/10.1267/ahc.29.243
9. Klinger MM, Rahemtulla F, Prince CW, Lucas LC, Lemons JE. Proteoglycans at the bone-implant interface. Crit Rev Oral Biol Med. 1998;9:449–63. https://doi.org/10.1177/10454411980090040401
10. Nakamura HK, Butz F, Saruwatari L, Ogawa T. A role for proteoglycans in mineralized tissue-titanium adhesion. J Dent Res. 2007;86:147–52. https://doi.org/10.1177/154405910708600208
11. Sugimoto K, Tsuchiya S, Omori M, Matsuda R, Fujio M, Kuroda K, et al. Proteomic analysis of bone proteins adsorbed onto the surface of titanium dioxide. Biochem Biophys Rep. 2016;7:316–22. https://doi.org/10.1016/j.bbrep.2016.07.007
12. Kamio H, Tsuchiya S, Kuroda K, Okido M, Okabe K, Ohta Y, et al. Chondroitin-4-sulfate transferase-1 depletion inhibits formation of a proteoglycan-rich layer and alters immunotolerance of bone marrow mesenchymal stem cells on titanium oxide surfaces. Acta Biomater. 2020;114:460–70. https://doi.org/10.1016/j.actbio.2020.07.034
13. Weber IT, Harrison RW, Iozzo RV. Model structure of decorin and implications for collagen fibrillogenesis. J Biol Chem. 1996;271:31767–70. https://doi.org/10.1074/jbc.271.50.31767
14. Jarvinen TA, Ruoslahti E. Target-seeking antifibrotic compound enhances wound healing and suppresses scar formation in mice. Proc Natl Acad Sci USA. 2010;107:21671–6. https://doi.org/10.1073/pnas.1016233107
15. Bini L, Schvartz D, Carnemolla C, Besio R, Garibaldi N, Sanchez JC, et al. Intracellular and extracellular markers of lethality in osteogenesis imperfecta: a quantitative proteomic approach. Int J Mol Sci. 2021. https://doi.org/10.3390/ijms22010429
16. Border WA, Ruoslahti E. Transforming growth factor-beta in disease: the dark side of tissue repair. J Clin Invest. 1992;90:1–7.
17. Danielson KG, Baribault H, Holmes DF, Graham H, Kadler KE, Iozzo RV. Targeted disruption of decorin leads to abnormal collagen fibril morphology and skin fragility. J Cell Biol. 1997;136:729–43. https://doi.org/10.1083/jcb.136.3.729
18. Bierbaum S, Douglas T, Hanke T, Scharnweber D, Tippelt S, Monsees TK, et al. Collageneous matrix coatings on titanium implants modified with decorin and chondroitin sulfate: characterization and influence on osteoblastic cells. J Biomed Mater Res A. 2006;77:551–62. https://doi.org/10.1002/jbm.a.30572
19. He R, Lu Y, Ren J, Wang Z, Huang J, Zhu L, et al. Decreased fibrous encapsulation and enhanced osseointegration in vitro by decorin-modified titanium surface. Colloids Surf B Biointerfaces. 2017;155:17–24. https://doi.org/10.1016/j.colsurfb.2017.03.055
20. Douglas T, Hempel U, Mietrach C, Heinemann S, Scharnweber D, Worch H. Fibrils of different collagen types containing immobilised proteoglycans (PGs) as coatings: characterisation and influence on osteoblast behaviour. Biomol Eng. 2007;24:455–8. https://doi.org/10.1016/j.bioeng.2007.07.008
21. Comalada M, Cardó M, Xaus J, Valledor AF, Lloberas J, Ventura F, et al. Decorin reverses the repressive effect of autocrine-produced TGF-beta on mouse macrophage activation. J Immunol. 2003;170:4450–6. https://doi.org/10.4049/jimmunol.170.9.4450
22. Arabpour M, Saghazadeh A, Rezaei N. Anti-inflammatory and M2 macrophage polarization-promoting effect of mesenchymal stem cell-derived exosomes. Int Immunopharmacol. 2021;97:107823. https://doi.org/10.1016/j.intimp.2021.107823
23. Kwon JH, Kim M, Bae YK, Kim GH, Choi SJ, Oh W, et al. Decorin secreted by human umbilical cord blood-derived mesenchymal stem cells induces macrophage polarization via CD44 to repair hyperoxic lung injury. Int J Mol Sci. 2019. https://doi.org/10.3390/ijms20194815
24. Gregory CA, Gunn WG, Peister A, Prockop DJ. An Alizarin red-based assay of mineralization by adherent cells in culture: comparison with cetylpyridinium chloride extraction. Anal Biochem. 2004;329:77–84. https://doi.org/10.1016/j.ab.2004.02.002
25. Dominici M, Le Blanc K, Mueller I, Slaper-Cortenbach I, Marini F, Krause D, et al. Minimal criteria for defining multipotent mesenchymal stromal cells. The International Society for Cellular Therapy position statement. Cytotherapy. 2006;8:315–7. https://doi.org/10.1080/14653240600855905
26. Ameye L, Young MF. Mice deficient in small leucine-rich proteoglycans: novel in vivo models for osteoporosis, osteoarthritis, Ehlers-Danlos syndrome, muscular dystrophy, and corneal diseases. Glycobiology. 2002;12:107R. https://doi.org/10.1093/glycob/cwf065
27. Wang M, Li Z, Zhang M, Wang H, Zhang Y, Feng Y, et al. Decorin knockdown affects the gene expression profile of adhesion, growth and extracellular matrix metabolism in C-28/I2 chondrocytes. PLoS ONE. 2020;15:e0232321. https://doi.org/10.1371/journal.pone.0232321

28. Mochida Y, Duarte WR, Tanzawa H, Paschalis EP, Yamauchi M. Decorin modulates matrix mineralization in vitro. Biochem Biophys Res Commun. 2003;305:6–9. https://doi.org/10.1016/s0006-291x(03)00693-4
29. Gu J, Wada Y. Effect of exogenous decorin on cell morphology and attachment of decorin-deficient fibroblasts. J Biochem. 1996;119:743–8. https://doi.org/10.1093/oxfordjournals.jbchem.a021304
30. D'Antoni ML, Risse PA, Ferraro P, Martin JG, Ludwig MS. Effects of decorin and biglycan on human airway smooth muscle cell adhesion. Matrix Biol. 2012;31:101–12. https://doi.org/10.1016/j.matbio.2011.11.001
31. Reed CC, Iozzo RV. The role of decorin in collagen fibrillogenesis and skin homeostasis. Glycoconj J. 2002;19:249–55. https://doi.org/10.1023/A:1025383913444
32. Zhang G, Chen S, Goldoni S, Calder BW, Simpson HC, Owens RT, et al. Genetic evidence for the coordinated regulation of collagen fibrillogenesis in the cornea by decorin and biglycan. J Biol Chem. 2009;284:8888–97. https://doi.org/10.1074/jbc.M806590200
33. Sharan J, Koul V, Dinda AK, Kharbanda OP, Lale SV, Duggal R, et al. Bio-functionalization of grade V titanium alloy with type I human collagen for enhancing and promoting human periodontal fibroblast cell adhesion - an in-vitro study. Colloids Surf B Biointerfaces. 2018;161:1–9. https://doi.org/10.1016/j.colsurfb.2017.10.024
34. Chen G, Deng C, Li YP. TGF-β and BMP signaling in osteoblast differentiation and bone formation. Int J Biol Sci. 2012;8:272–88. https://doi.org/10.7150/ijbs.2929
35. Wu M, Chen G, Li YP. TGF-β and BMP signaling in osteoblast, skeletal development, and bone formation, homeostasis and disease. Bone Res. 2016;4:16009. https://doi.org/10.1038/boneres.2016.9
36. Zhang W, Ge Y, Cheng Q, Zhang Q, Fang L, Zheng J. Decorin is a pivotal effector in the extracellular matrix and tumour microenvironment. Oncotarget. 2018;9:5480–91. https://doi.org/10.18632/oncotarget.23869
37. Steen EH, Wang X, Balaji S, Butte MJ, Bollyky PL, Keswani SG. The role of the anti-inflammatory cytokine interleukin-10 in tissue fibrosis. Adv Wound Care. 2020;9:184–98. https://doi.org/10.1089/wound.2019.1032